C. R. Chimie 20 (2017) 385–394

Contents lists available at ScienceDirect

Comptes Rendus Chimie

www.sciencedirect.com

Full paper/Mémoire

Synthesis of ZSM-5 aggregates by a seed-induced method and catalytic performance in methanol-to-gasoline conversion

Fanjun Meng, Yaquan Wang*, Shougui Wang, Xiao Wang, Shuhai Wang

Key Laboratory for Green Chemical Technology of the Ministry of Education, School of Chemical Engineering & Technology, Tianjin University, Tianjin 300072, PR China

ARTICLE INFO

Article history:
Received 28 April 2016
Accepted 18 July 2016
Available online 27 August 2016

Keywords:
ZSM-5 aggregates
Na_2O/SiO_2
H_2O/SiO_2
MTG

ABSTRACT

A seed-induced method was applied to synthesize a series of ZSM-5 aggregates using silicalite-1 (S-1) as seeds. The samples were characterized by several techniques and studied in the methanol-to-gasoline (MTG) conversion reaction in a continuous fixed-bed reactor. The results showed that the molar ratios of Na_2O/SiO_2 and H_2O/SiO_2 in the precursors had great effects on the physicochemical and catalytic properties. The ZSM-5 aggregates with the highest crystallinity, external surface areas, micropore volumes, mesopore volumes and small primary crystal and aggregate sizes, obtained with the molar composition of $0.12Na_2O-1SiO_2-0.02Al_2O_3-25H_2O$-0.01Seed in the precursor, exhibited the highest stability.

1. Introduction

Gasoline, as the most important transportation fuel in the world, is conventionally obtained from the cracking of crude oil. However, as the increase of energy demands and the depletion of crude oil reservoirs, the exploration of new routes to obtain gasoline from some substitutions of crude oil becomes a hot and endless topic [1,2]. Methanol-to-gasoline (MTG) has been proven to be an ideal process to offer a desired solution for the production of gasoline because methanol can be easily manufactured from biomass, natural gas and coal [3,4].

A ZSM-5 zeolite is a kind of crystalline aluminosilicate which has two interconnected pore systems, *i.e.* zigzag channels (0.53 nm × 0.56 nm) and straight channels (0.51 nm × 0.55 nm), creating a three-dimensional network [5]. ZSM-5 zeolites have exhibited excellent catalytic properties in MTG due to the strong acid sites and the regular nanochannel system [6–9] and have been proved to be the most proper catalyst in the MTG process [10,11]. When contacting with ZSM-5 zeolites, methanol is converted into hydrocarbons with the similar fractions to traditional gasoline. In 1977, Exxon Mobil successfully commercialized the methanol to gasoline process with ZSM-5 zeolites as catalysts [12].

Since it was first reported by Mobil in 1972 [13], the hydrothermal syntheses of ZSM-5 zeolites with one or more organic templates have been widely studied [6,14–19]. Many efforts have also been made in attempting to generate mesopores in the zeolites by using mesoscale templates, such as cationic polymers, amphiphilic organosilane, *etc.*, and many of them have been successfully applied in the reaction of MTG [5,20–22]. However, the use of organic templates is not appreciated in the point view of both the economics and the environmental protection. Moreover, elevated temperature is needed to remove the templates, which results in the aggregation of the primary crystals [23]. To obtain hierarchical ZSM-5 with mesopores, the method of post-treatment such as dealumination or desilication was also used [24,25]. However, they are generally limited by the partial damage of the framework and sometimes the blockage of the micropores by the extra-framework residue generated during the

* Corresponding author.
E-mail address: yqwang@tju.edu.cn (Y. Wang).

http://dx.doi.org/10.1016/j.crci.2016.07.005
1631-0748/

hydrothermal treatment and chemical extraction [26]. To overcome the disadvantages of the methods for obtaining hierarchical ZSM-5 mentioned above, several strategies for preparing ZSM-5 zeolites with a hierarchical structure by seed-induced methods without organic templates or post-treatments have been proposed. The ZSM-5 zeolites synthesized by a seed-induced method have been applied in many reactions, for example, the alkylation of naphthalene [27], cyclohexene hydration [28], methanol-to-hydrocarbon [29], methanol-to-olefin [30], propane dehydrogenation [31,32], *etc*. In some reactions above, excellent catalytic performances of the hierarchical ZSM-5 were obtained because the ZSM-5 zeolites were aggregates of nanosized particles which reserve the advantages of low diffusion limitation, large external surface area, large mesopore volume, *etc*. The influence of alkalinity (Na_2O/H_2O) and aging conditions on the crystal morphology, crystallinities and elemental component of ZSM-5 in the seed-induced method has been reported [33,34]. However, the zeolites were not evaluated for any catalytic reactions. Although Zhang et al. [35] obtained mesopore-containing ZSM-5 zeolites by using a coke-deposited spent zeolite catalyst. In the methanol to propylene reaction, the refabricated ZSM-5 catalyst exhibited much higher propylene selectivity and a longer catalytic lifetime. To the best of our knowledge, few have reported the reaction of MTG over ZSM-5 synthesized by the seed-induced methods.

In this work, hierarchical ZSM-5 aggregates were synthesized by a seed-induced method with S-1 crystals as the seeds. The molar ratios of Na_2O/SiO_2 and H_2O/SiO_2 in the synthesis that markedly influenced the properties of the zeolites were investigated in detail. The samples were characterized by many techniques and studied in the MTG reaction. The ZSM-5 aggregates showed excellent catalytic performance and were correlated with the physicochemical properties.

2. Experimental

2.1. Materials

Tetraethyl orthosilicalite (TEOS, AR) was purchased from Tianjin Kemiou Chemical Reagent Co., China. Sodium aluminates ($NaAlO_2$, AR), sodium hydroxide (NaOH, AR), methanol (MeOH, AR) and commercial HZSM-5 (SiO_2/Al_2O_3 = 50) were purchased from Tianjin Guangfu Chemical Reagent Co., China. Silica gel of 40% SiO_2 in water (AR) was purchased from Qingdao Haiyang Chemical Reagent Co., China. Hydrochloric acid (HCl, AR) was purchased from Tianjin Jiangtian Chemical Reagent Co., China. All purchased chemicals were used without further purification. Tetrapropyl ammonium hydroxide was prepared through ion-exchange of tetrapropyl ammonium bromide.

2.2. Preparation of seed S-1

S-1 was synthesized by a hydrothermal method. TEOS was added dropwise into an aqueous solution of 15 wt % TPAOH. The molar composition was $100SiO_2$–$400EtOH$–$24TPAOH$–$2400H_2O$ in which EtOH was produced from the hydrolysis of TEOS. The mixture was stirred (600 rpm) at ambient temperature for 3 h, and then transferred into a Teflon-lined autoclave. The hydrothermal treatment was performed at 105 °C for 48 h [36–38]. The obtained S-1 nanocrystals suspended in the mother liquor were directly used as the seed.

2.3. Synthesis of ZSM-5 by the seed-induced method

The synthesis of ZSM-5 with the molar composition xNa_2O–$1SiO_2$–$0.02Al_2O_3$–yH_2O–0.01Seed (x = 0.08, 0.10, 0.12, 0.14, 0.16, y = 25, 35, 45, 55) was started by adding a 3 M NaOH solution to a 0.3 M $NaAlO_2$ solution, stirred at room temperature for 15 min before the S-1 suspension was introduced. Then the silica gel solution was slowly dropped into the mixture under vigorous stirring (600 rpm). The solution was stirred at room temperature for another 2 h before being transferred into a Teflon-lined autoclave and hydrothermally treated at 170 °C for 10 h. After cooling, the product was recovered by filtration and washed with deionized water until the pH reached 8 [23,38–40]. Finally, the as-synthesized samples were ion-exchanged with 0.5 M HCl solution at 90 °C for 2 h, followed by washing, drying and calcination at 550 °C for 6 h. The samples were denoted as ZM-x-y, where x and y refer to the molar ratios of Na_2O/SiO_2 and H_2O/SiO_2 in the precursors, respectively.

2.4. Characterization

The X-ray powder diffraction (XRD) patterns of ZSM-5 were obtained on a Bruker D8-Focus diffractometer with Cu Kα radiation at a scanning rate of 8°/min in the 2θ range of 5–55°. The relative crystallinities were estimated by comparing the total intensity of the characteristic peaks (between 2θ = 22° and 24°) with the sample with the highest crystallinity. Scanning electron microscopy (SEM) images were recorded using a Hitachi S-4800 microscopy. N_2 adsorption and desorption isotherms were measured at −196 °C on a Micromeritics TriStar 3000 instrument. SiO_2/Al_2O_3 ratios were measured on a Bruker-axs S4 Explorer X-ray fluorescence spectroscope (XRF). NH_3-TPD measurements were carried out by using a TP-5076 instrument supplied by Tianjin Xianquan Co. to measure the amounts of acid sites and acid strength of the catalysts. The amounts of the deposited materials after the reaction were determined with a Shimadzu TGA-50 thermogravimetric analyzer. The samples were combusted in the flow of air from room temperature to 700 °C with a ramp of 10 °C/min and the weight loss between 300 and 700 °C was attributed to the burning of the deposit [40].

2.5. Catalyst evaluation for MTG

The MTG reaction was carried out at atmospheric pressure in a quartz tube fixed bed reactor with an internal diameter of 10 mm and a total length of 370 mm. In a typical run, the reactor was packed with 0.5 g catalyst which was sieved to 425–850 μm and diluted with quartz particles of the same sizes in a 1:2 volume ratio. The catalyst was pretreated in situ at 400 °C for 2 h with a heating rate of 10 °C/min in the flow of 50 cm^3/min N_2. Then liquid methanol was fed into the reactor at a weight

hourly space velocity (WHSV) of 10 h^{-1} with a micropump. The reaction temperature was maintained at 400 °C. The products were separated with an ice-cooled condenser. The gas products were analyzed on a gas chromatograph (GCSP-3420A) equipped with a flame ionization detector (FID) and a KB-PLOT Q (50 m × 0.32 mm × 10 μm) capillary column. The liquid products were analyzed on another gas chromatograph (GCSP-3420A) equipped with an FID and an SE-54 (30 m × 0.25 mm × 0.33 μm) capillary column. The methanol conversion was calculated by the following equation:

$$\text{methanol conversion}(\%) = (M_{in} - M_{out} - 2M_{DME,out}) / M_{in} \times 100 \quad \text{(a)}$$

where M_{in}, M_{out} and $M_{DME,out}$ denoted the amounts of pumped in, unconverted methanol and the produced dimethylether during the reaction, respectively.

The naming conversions were used in calculating the product selectivities: C_{1-4} represented the gaseous hydrocarbons with carbon numbers ranging between 1 and 4; TMB referred to trimethylbenzene; C_{5+} was the sum of hydrocarbons with carbon numbers ≥5 (benzene, toluene, xylene and TMB were excluded). The product selectivities were calculated using the following equation:

$$\text{product selectivity}(\%) = M_i / M_{HC} \times 100 \quad \text{(b)}$$

where M_i was the amount of the product to be calculated and M_{HC} was the total amount of hydrocarbon products.

3. Results and discussion

3.1. Characterization of samples with different ratios of Na_2O/SiO_2 and H_2O/SiO_2

XRD patterns of ZSM-5 with different ratios of Na_2O/SiO_2 and H_2O/SiO_2 in the synthesis mixture are presented in Fig. 1. Five typical diffraction peaks of the MFI framework appeared without other peaks, confirming a high purity of the products. The relative crystallinities, with the highest of ZM-0.12-25 being taken as 100%, are shown in Table 1.

As shown in Fig. 1A, with the increase of Na_2O/SiO_2 ratios in the precursors, the peak intensities of the obtained ZSM-5 first increased and then decreased. For the sample of ZM-0.08-25, the low ratio of Na_2O/SiO_2 means that less Na^+ ions were introduced into the precursor species. According to the literature [34,41], in obtaining MFI type zeolites, Na^+ ions play a very important role which can direct the MFI structure, stabilize the formation of structural submits and favor the formation of secondary building units needed for the nucleation and the crystallization of ZSM-5 zeolites. Due to the low Na_2O/SiO_2 ratio of 0.08, ZM-0.08-25 did not crystallize completely under the synthesis conditions (hydrothermal treatment at 170 °C for 10 h), therefore the intensities of the peaks were weak. At the same time, the dissolution of silica by OH^- ions is an important process, and more OH^- ions in the precursors lead to the easy formation of aluminasilicate and thus the growth of crystals [42]. In the precursors of ZM-0.08-25, also due to the low concentration of OH^- ions, silica might not have been completely dissolved by OH^- ions under the given conditions, which contributed to the appearance of amorphous materials in the end products. So, with the increase of the Na_2O/SiO_2 ratios in the precursors, the peak intensities of the obtained ZSM-5 first increased. However, too many OH^- ions make a deeper depolymerization of aluminasilicate occur [42]. Thus the degree of the crystallization decreased with further increase of the Na_2O/SiO_2 ratios. As shown in Fig. 1B, the peak intensities of the samples decreased gradually with increasing the H_2O/SiO_2 ratios in the precursors. This should be ascribed to the decrease of Na^+ and OH^- ion concentrations by adding more H_2O in the synthesis.

SEM was applied to investigate the morphology and particle sizes of the samples as well as the crystals combined in the aggregates. Fig. 2A shows that the seed S-1 had an irregular sphere morphology with the crystal sizes of *ca.* 150 nm. As seen in Fig. 2B–F, typical shapes of both the aggregates and the crystals strongly depended on the Na_2O/SiO_2 ratios in the synthesis mixture. With increasing the Na_2O/SiO_2 ratios from 0.08 to 0.16, the aggregate size decreased from 1 μm to 0.6 μm; however, the primary crystal size first decreased from ca. 700 nm

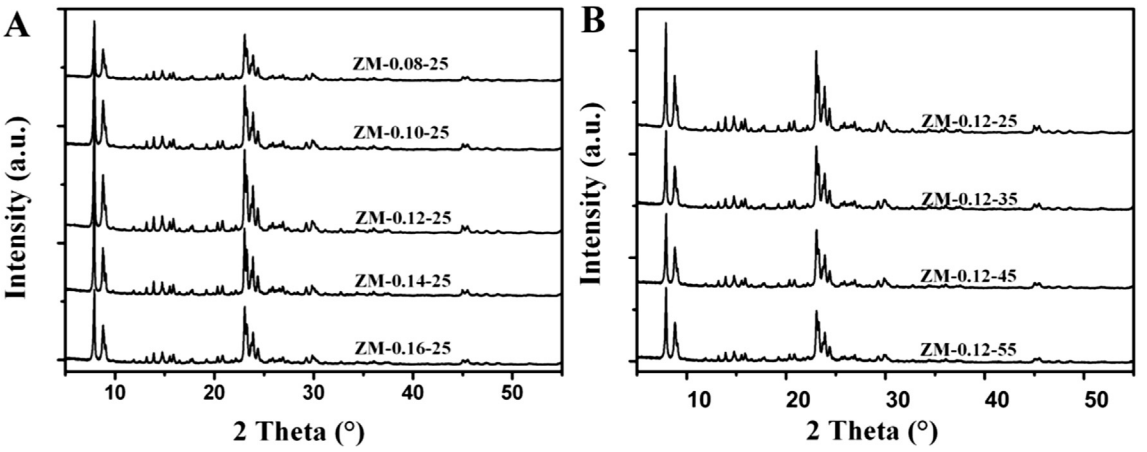

Fig. 1. XRD patterns of ZSM-5 with different ratios of Na_2O/SiO_2 and H_2O/SiO_2 in the synthesis mixture.

Table 1
Textural properties of ZSM-5 with different ratios of Na_2O/SiO_2 and H_2O/SiO_2.

Sample	Relative crystallinity	Surface area (m^2/g)			Pore volumes (cm^3/g)		
		S_{BET}[a]	S_{Micro}[b]	S_{Ext}[b]	V_{Total}[c]	V_{Micro}[b]	V_{Meso}[d]
ZM-0.08-25	56	287	224	63	0.158	0.103	0.055
ZM-0.10-25	79	321	248	74	0.179	0.113	0.066
ZM-0.12-25	100	330	252	78	0.193	0.117	0.076
ZM-0.14-25	82	310	246	64	0.180	0.113	0.067
ZM-0.16-25	70	305	251	54	0.162	0.116	0.046
ZM-0.12-35	88	322	249	72	0.184	0.118	0.066
ZM-0.12-45	76	310	246	64	0.165	0.113	0.052
ZM-0.12-55	65	262	215	47	0.145	0.099	0.046

[a] Calculated by the BET method in the p/p_0 range of 0.01–0.1.
[b] Calculated using the *t*-plot method.
[c] Calculated by measuring the amount of adsorbed nitrogen at $p/p_0 = 0.99$.
[d] Calculated using $V_{Total}-V_{Micro}$.

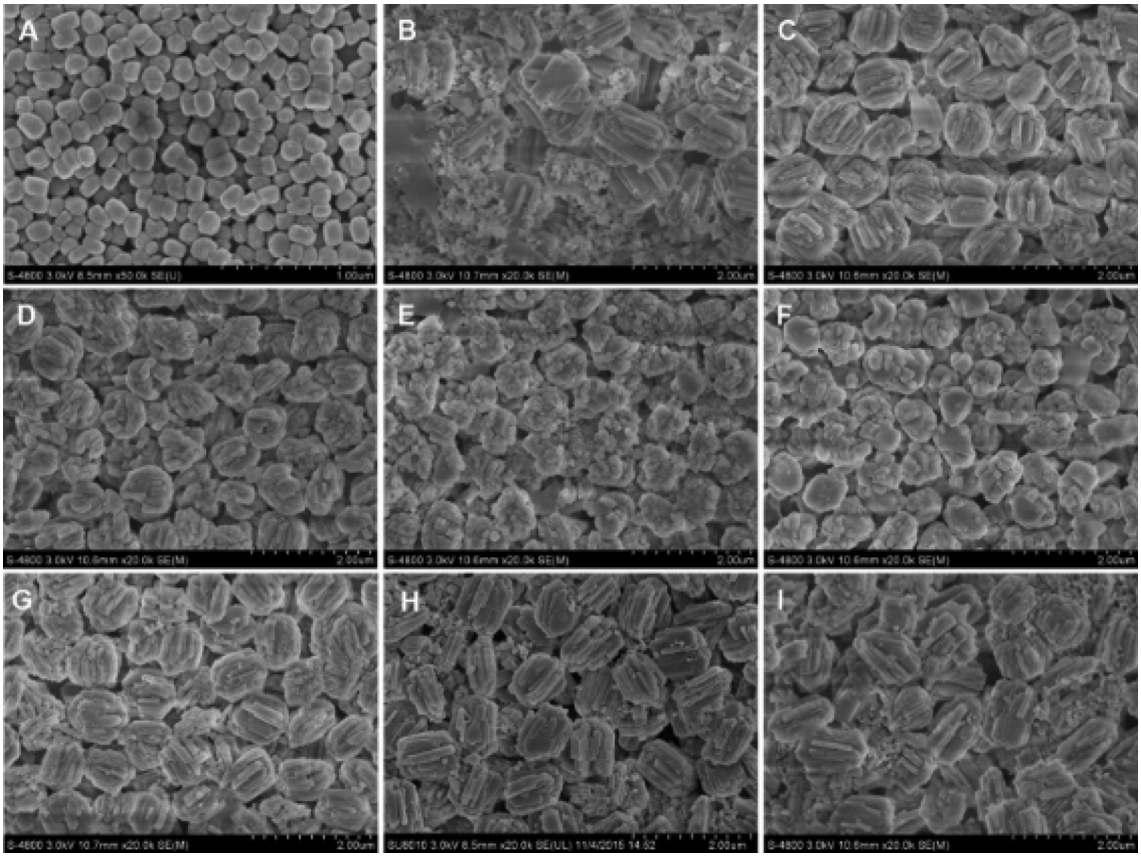

Fig. 2. SEM images of (A) S-1, (B) ZM-0.08-25, (C) ZM-0.10-25, (D) ZM-0.12-25, (E) ZM-0.14-25, (F) ZM-0.16-25, (G) ZM-0.12-35, (H) ZM-0.12-45, and (I) ZM-0.12-55.

of ZM-0.08-25 to ca. 200 nm of ZM-0.14-25, and then increased to ca. 500 nm of ZM-0.16-25. With increasing the Na_2O/SiO_2 ratios, the coffin crystals in ZM-0.08-25 gradually disappeared and became small spherical nanocrystals. At the same time, the crystallization did not complete and there were some amorphous materials between the zeolite crystals. The sample with the smallest nanocrystals of 80 nm appeared in ZM-0.14-25. The aggregates with uniform sizes of ca. 800 nm composing of 200–400 nm nanocrystals were formed in ZM-0.12-25 without impurities.

Apart from the contribution of Na^+ ions to the nucleation and crystal growth [34,41,43], OH^- ions could dissolve the surfaces of S-1 seeds and release some ingredients which could be the nuclei for the formation of small crystals [42]. At the end, the seeds were attached by small particles due to the high surface Gibbs free energy [27]. With the continuous increase of OH^- ions, some of the

small crystals might be dissolved and larger crystals were obtained as shown in the SEM images of ZM-0.14-25 and ZM-0.16-25. This phenomenon could be ascribed to the reason that zeolite crystallization, being similar to other crystallization processes, was accompanied by Ostwald ripening, which is a spontaneous and natural process, and can minimize the surface free energy of crystals by dissolving small crystals and contribute to large crystal growth [22,44,45]. In addition, it should be recalled that the mechanism of the crystallization was different from that suggested by Ren et al. who synthesized well faceted ZSM-5 and put forward a seed surface crystallization (SSC) mechanism [38]. In this work, the seeds might be dissolved releasing some ingredients which induced the growth of small crystals attached on the seeds, and the mechanism was similar to that of Xue et al. [26]. To track the structural changes in the synthesis, the sample with the same components of ZM-0.12-25 was hydrothermally crystallized for different times. The SEM images (in Fig. S1) showed that after crystallization for 5 h, there were some amorphous materials attached on the surfaces of S-1. With the prolonging of the crystallization time, the aluminasilicate transformed into a zeolite and after 7 h the aggregates appeared. After crystallization for 10 h, the products were dominated by zeolite aggregates consisting of clear primary crystals, while no amorphous phase could be observed.

The SEM images of samples with different molar ratios of H_2O/SiO_2 (25, 35, 45 and 55) are presented in Fig. 2D, G, H and I, respectively. With increasing the H_2O/SiO_2 ratios, the aggregate sizes increased and the small spherical individual crystals were replaced by bigger coffin or thick sheet shaped individual ones. At the same time, there were some amorphous materials appeared between the aggregates at the H_2O/SiO_2 molar ratio $\geq$35. Increasing the ratios of H_2O/SiO_2 reduced the concentrations of both Na^+ and OH^- ions, decreasing the crystal growth rate and gradually preventing the dissolution of S-1 and/or ZSM-5 crystals; therefore well-defined large crystals were formed on the surfaces of the seeds.

The N_2 adsorption/desorption isotherms of the samples with different ratios of Na_2O/SiO_2 and H_2O/SiO_2 are presented in Fig. 3, and the corresponding textural properties are also listed in Table 1. All the samples exhibited type IV isotherms with hysteresis loops. The hysteresis loops of ZM-0.08-25 and ZM-0.16-25 were slightly discernable. The hysteresis loops appearing in the isotherms at the relative pressure of $p/p_0 > 0.5$ were usually associated with the capillary condensation taking place in the mesopores. The shapes of the hysteresis loops displayed an H3 type (loosely packed pores), confirming the formation of mesopores resulted from the voids constructed upon the aggregation of individual crystals [27,28,31].

With increasing the Na_2O/SiO_2 ratios, the BET specific surface areas, micropore surface areas, mesopore surface areas, total volumes, micropore volumes and mesopore volumes generally first increased and then decreased, and at a Na_2O/SiO_2 ratio of 0.12, the peak values appeared. The variations of the values were in accordance with their N_2 adsorption/desorption isotherms and could be ascribed to the differences of the sample morphologies. With the increase of the Na_2O/SiO_2 ratios, the primary crystal sizes decreased and then increased; therefore the amounts of voids constructed upon the aggregation of individual crystals first increased and then decreased, which led to the variations of isotherms and the corresponding textural properties. With the increase of H_2O/SiO_2 ratios, all the samples exhibited isotherms of type IV with H3 type hysteresis loops; the hysteresis loops became smaller and smaller; the BET specific surface areas, micropore surface areas, mesopore surface areas, total volumes, micropore volumes and mesopore volumes all decreased gradually. All the results above could be ascribed to the increase of the aggregates and primary crystal sizes in the four samples.

XRF analyses of all the samples are shown in Table 2. With the increase of Na_2O/SiO_2 ratios, the ratios of SiO_2/Al_2O_3 decreased from 48.7 to 37.5. There are two main factors affecting the SiO_2/Al_2O_3 ratios, *i.e.* the concentration of OH^- ions and Na^+ ions. The OH^- ions can contribute to

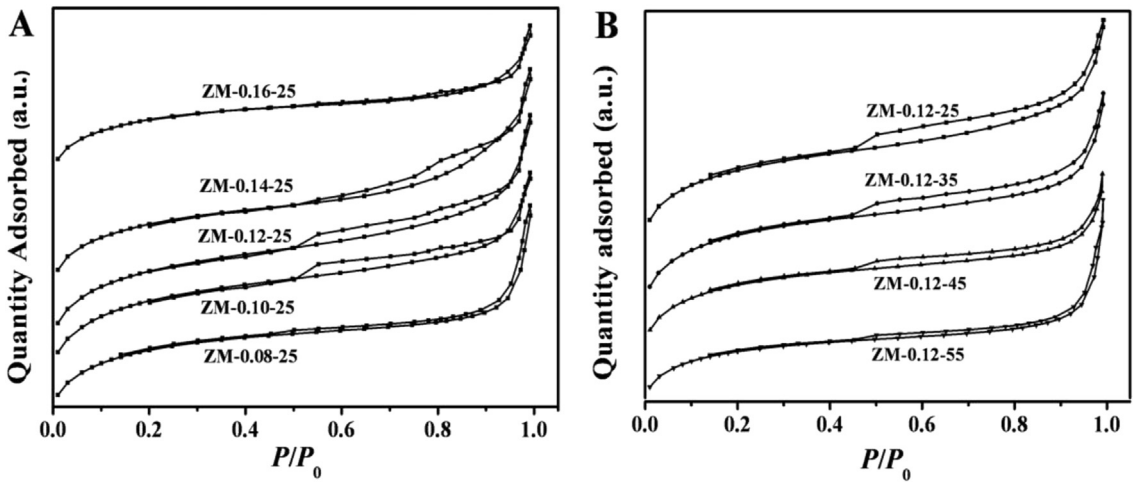

Fig. 3. N_2 adsorption/desorption isotherms of samples with different ratios of Na_2O/SiO_2 and H_2O/SiO_2 at −196 °C.

Table 2
Elemental component and acid amounts of the samples.

Samples	Elemental component (SiO_2/Al_2O_3)[a]	Acid amounts (mmol/g)[b]		
		Total acidity	Weak acidity	Strong acidity
ZM-0.08-25	48.7	0.602	0.405	0.197
ZM-0.10-25	46.1	0.629	0.419	0.210
ZM-0.12-25	43.5	0.664	0.431	0.233
ZM-0.14-25	40.4	0.716	0.447	0.259
ZM-0.16-25	37.5	0.817	0.553	0.264
ZM-0.12-35	44.0	0.721	0.433	0.288
ZM-0.12-45	44.2	0.503	0.292	0.211
ZM-0.12-55	46.1	0.588	0.433	0.155

[a] Determined by XRF.
[b] Calculated by NH_3-TPD.

the dissolution of amorphous silica in the synthesis mixture. With the increase of Na_2O/SiO_2 ratios, more OH^- ions were introduced into the mixture, which facilitated the dissolution of more amorphous silica and then the crystallization rate. Hence the SiO_2/Al_2O_3 ratios of the samples increased. However, enhancing the Na_2O/SiO_2 ratios means that more Na^+ ions are also introduced into the synthesis mixture. As charge compensators, Na^+ ions can keep the balance of the charges for the framework of ZSM-5 and facilitate the introduction of aluminum into the framework [34]. Therefore, with the increase of Na_2O/SiO_2 ratios, the amounts of aluminum in the end products should increase. In general, as the Na_2O/SiO_2 ratios increased, the ratios of SiO_2/Al_2O_3 decreased. The higher the H_2O/SiO_2 ratios in the precursors, the higher the SiO_2/Al_2O_3 ratios of the samples. It can be seen in the SEM images (Fig. 2) that, with the increase of H_2O/SiO_2 ratios, there were increasing amounts of amorphous materials between the aggregates, which might be amorphous silicate; therefore the SiO_2/Al_2O_3 ratios detected by XRF increased slightly.

NH_3-TPD diagrams of the samples are presented in Fig. 4, and the related data are listed in Table 2. The TPD desorption peaks were in the ranges of 193–208 °C and 420–440 °C which were attributed to the chemical desorption of NH_3 from weak and strong acidic sites, respectively. As shown in Table 2, the increase of Na_2O/SiO_2 ratios in the precursors increased the amounts of both the weak and the strong acid sites. The numbers of the total acid sites decreased with the increase of the H_2O/SiO_2 ratios. The acid sites are caused by the incorporation of the aluminum into zeolites; therefore the change of the aluminum contents in the products led to the variations of the amounts of the total acid sites [46].

3.2. Catalyst performance in MTG

The methanol conversions and yields of light hydrocarbons (LHs) as a function of time on stream over the catalysts with different Na_2O/SiO_2 ratios are given in Fig. 5. It should be reiterated that in order to compare the catalysts quickly, the reactions were conducted at high WHSV (10 h^{-1}) [10]. ZM-0.08-25 had the lowest stability. With increasing the Na_2O/SiO_2 ratios in the synthesis, the stability of the samples increased. At a Na_2O/SiO_2 ratio of 0.12, the sample ZM-0.12-25 had the highest stability. When the Na_2O/SiO_2 ratios were increased further, the stability of the samples decreased. The characterization results showed that compared with the other catalysts, ZM-0.12-25 had relatively small aggregates and primary crystals, the highest external surface areas and the largest mesopore volumes, which could provide easy accessibility of the reactants to the acid sites [47–52] and reduce the diffusion limitations for large molecules, avoiding severe coking. Fig. 6A depicts the thermalgravity analysis (TGA) profiles of the samples with different Na_2O/SiO_2 ratios after the reaction time of 12 h. With increasing the Na_2O/SiO_2 ratios, the amounts of coke formed in the catalysts first decreased and then increased. ZM-0.12-25 had the highest resistance to coking, which could be attributed to the highest stability. Moreover, its highest crystallinity might also contribute to the best performance.

With increasing the Na_2O/SiO_2 ratios, the SiO_2/Al_2O_3 ratios decreased slightly. However, the variation of the SiO_2/Al_2O_3 ratios in the zeolite synthesized under the conditions for ZM-0.12-25 had meager influence on the performance in MTG (see the Supporting information). So, the excellent performance of ZM-0.12-25 was not caused by

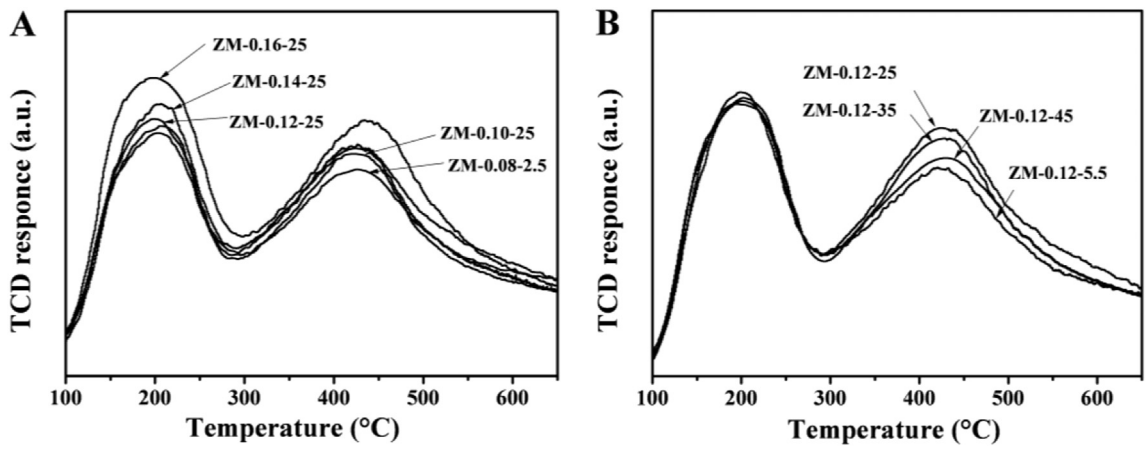

Fig. 4. NH_3-TPD spectra of the samples with different ratios of Na_2O/SiO_2 and H_2O/SiO_2.

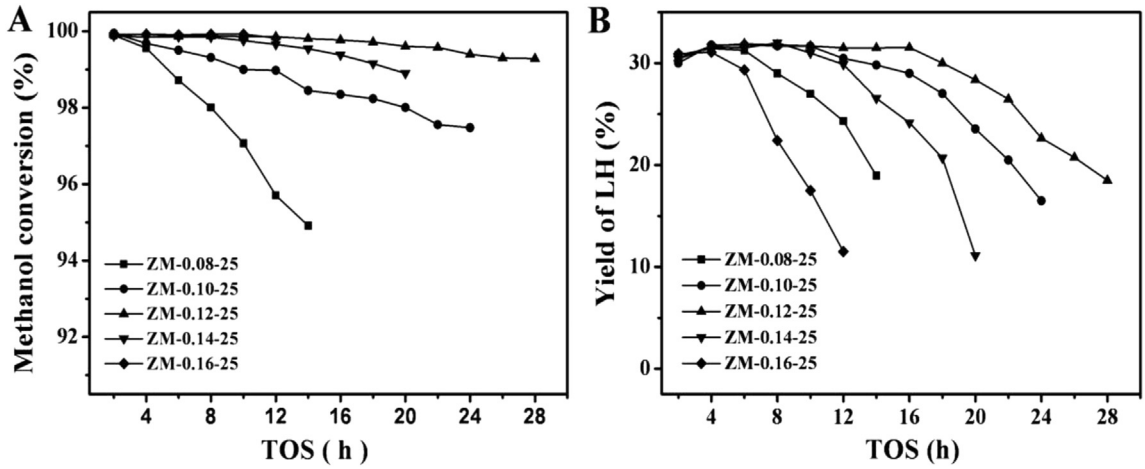

Fig. 5. Catalytic performance of the prepared catalysts with different Na_2O/SiO_2 ratios. (A) The methanol conversions and (B) the LH yields. Reaction conditions: 400 °C, 1 atm, and WHSV = 10 h^{-1}.

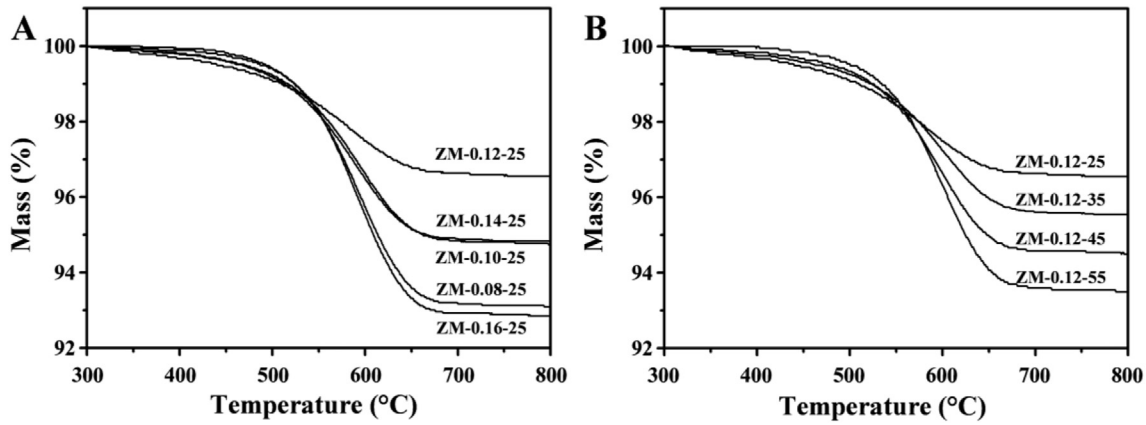

Fig. 6. TGA profiles of the catalyst samples after undergoing 12 h under the same reaction conditions: 400 °C, 1 atm, and WHSV = 10 h^{-1}.

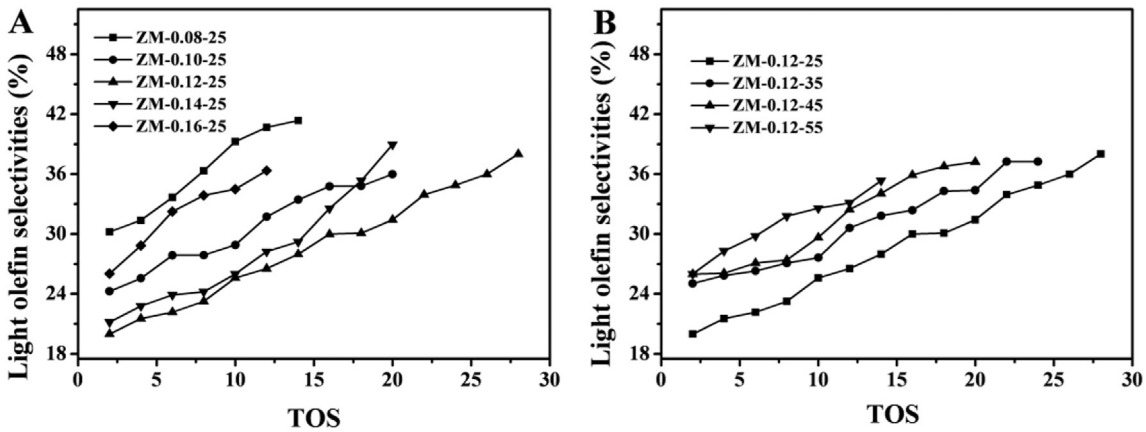

Fig. 7. Total selectivities of light olefins versus time on stream. Reaction conditions: 400 °C, 1 atm, and WHSV = 10 h^{-1}.

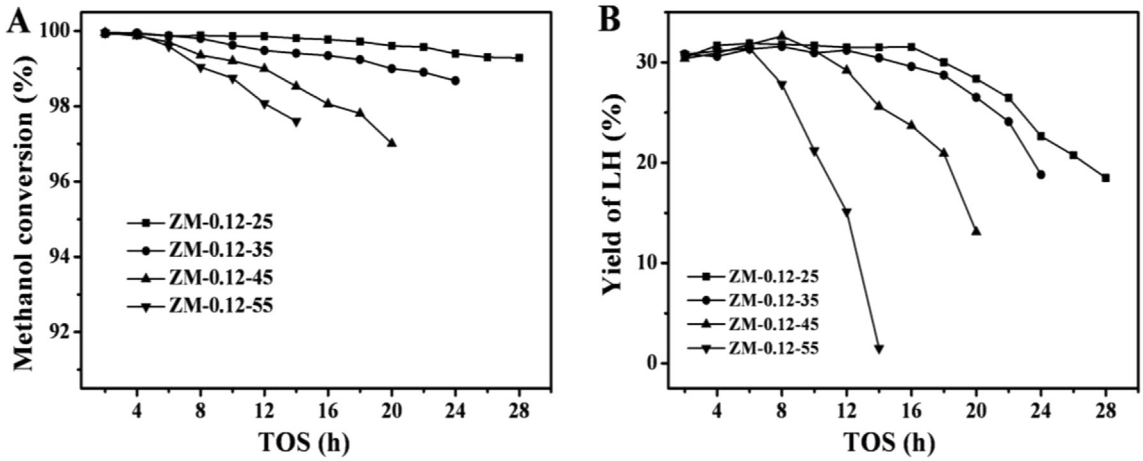

Fig. 8. Catalytic performance of the prepared catalysts with different H_2O/SiO_2 ratios. (A) The methanol conversions and (B) the LH yields. Reaction conditions: 400 °C, 1 atm, and WHSV = 10 h^{-1}.

the variation of SiO_2/Al_2O_3 ratios with the change of the Na_2O amount in the synthesis.

As shown in Fig. 5B, all the samples exhibited constant yields of LHs (ca. 32%) during the stable time on stream, but decreased when the conversions decreased. The total selectivities of the light olefins (ethylene C_2=, propylene C_3= and butylene C_4=) with time on stream over the samples are shown in Fig. 7A. The selectivities of the light olefins over ZM-0.12-25 were the lowest, which might result from the reason that most of the methanol was converted to gasoline.

The methanol conversions with time on stream over the samples with different H_2O/SiO_2 ratios are shown in Fig. 8A. All the samples showed almost the same initial methanol conversions of 100%. The methanol conversion over ZM-0.12-25 remained the highest during the time on stream, *i.e.* after 28 h of the reaction the conversion remained at 98%. The increase of the H_2O/SiO_2 ratios in the synthesis resulted in the faster deactivations as certified by TGA in Fig. 6B, which might result from the increase of the zeolite aggregate and the primary crystal sizes as well as the decrease of the total surface areas, external surface areas and mesopore volumes.

As shown in Fig. 8B, during the initial reaction period, the four samples had the same LH yields (ca. 32%) at the initial time, but then decreased with the time on stream. This might result from the fact that the acid sites of the samples were enough for the reaction at the initial time, but then decreased due to coking. The total selectivities of the light olefins (C_2=, C_3= and C_4=) with time on stream over the samples are shown in Fig. 7B. The selectivities of the light olefins over ZM-0.12-25 were the lowest, which might result from the reason that most of the methanol was converted to gasoline.

Among all the catalysts, ZM-0.12-25 exhibited the best performance in MTG. Compared with the commercial ZSM-5 (Fig. S2), the lifetime of ZM-0.12-25 increased by a factor of 2.

Table 3 lists the methanol conversions and hydrocarbon selectivities for the MTG reactions over the synthesized catalysts at a TOS of 6 h. The product distributions of the reactions over the samples with different Na_2O/SiO_2 and H_2O/SiO_2 ratios did not show much significant difference. This might result from the fact that in the first several hours of the reaction, the active sites, *i.e.* acid sites, on the surface of the catalysts were enough for the conversion and were not the rate-determining factors. The selectivities of the different light olefins compared at a TOS of 6 h are shown in Fig. 9. The components of the light olefins were similar, but the total amount of the light olefins over ZM-0.12-25 was the lowest, which might result from the reason that most of the methanol was converted to gasoline.

In the synthesis of the hierarchical ZSM-5 aggregates by the seed-induced method, samples with different molar

Table 3
Methanol conversion and hydrocarbon distribution (TOS = 6 h, 400 °C, 1 atm, and WHSV = 10 h^{-1}).

Sample	Methanol conversion (%)	Selectivity (%)						Yield of LH (%)
		C_{1-4}	C_{5+}	C_{bene}	$C_{toluene}$	C_{xylene}	C_{TMB}	
ZM-0.08-25	98.7	46.7	26.4	1.1	7.7	12.5	5.6	31.3
ZM-0.10-25	99.5	47.2	30.7	1.2	7.6	13.1	6.5	31.8
ZM-0.12-25	99.9	46.9	31.5	1.5	7.6	12.4	6.6	31.9
ZM-0.14-25	99.9	47.6	31.1	1.5	7.2	12.7	5.6	31.5
ZM-0.16-25	99.9	46.6	31.9	1.5	7.6	12.3	5.1	29.3
ZM-0.12-35	99.9	47.5	31.4	1.4	7.4	12.3	6.2	31.3
ZM-0.12-45	99.7	44.5	31.3	1.3	7.2	12.6	6.0	31.8
ZM-0.12-55	99.6	46.1	31.1	1.2	7.6	11.3	5.5	31.4

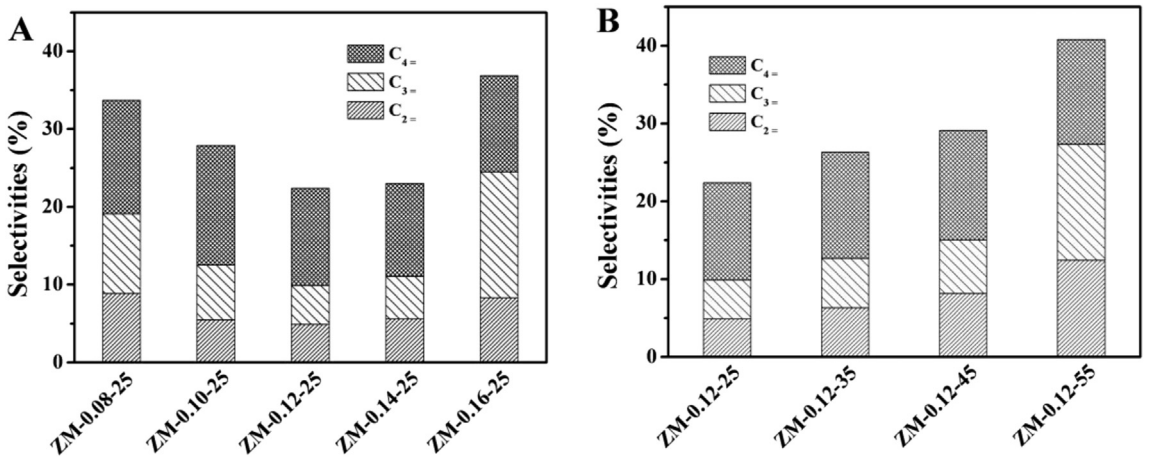

Fig. 9. Selectivities toward the different light olefins compared at TOS = 6 h for the samples. Reaction conditions: 400 °C, 1 atm, and WHSV = 10 h^{-1}.

ratios of SiO_2/Al_2O_3 and seed/SiO_2 had also been studied. The results in Fig. S3–6 in the supplements showed that the samples with different molar ratios of SiO_2/Al_2O_3 and seed/SiO_2 had meager effects on the catalytic performance in the MTG reaction. However, the ratios of Na_2O/SiO_2 and H_2O/SiO_2 had pronounced effects on the final products as discussed above.

4. Conclusions

Hierarchical ZSM-5 aggregates had been successfully synthesized using a seed-induced method without adding organic templates and studied in the reaction of MTG. The hierarchical ZSM-5 zeolites were aggregates of small crystals. Among the parameters studied, the ratios of Na_2O/SiO_2 and H_2O/SiO_2 in the synthesis mixture had pronounced influence on the physicochemical properties of the samples and thus the performances in MTG.

With increasing the Na_2O/SiO_2 ratios from 0.08 to 0.16, the aggregate sizes decreased from 1 μm to 0.6 μm. The aggregates with the highest crystallinity, uniform primary crystals (200–400 nm), the highest total surface areas, the highest external surface areas, and the largest micropore volumes and mesopore volumes were obtained at a Na_2O/SiO_2 ratio of 0.12 (sample ZM-0.12-25). When applied in the reaction of MTG, ZM-0.12-25 also exhibited the longest lifetime.

The increase of the H_2O/SiO_2 ratio in the precursors led to the decrease of the crystallinity, total specific surface areas, external surface areas, micropore volumes, mesopore volumes and the amounts of aluminum in the framework of the zeolite. In the reaction of MTG, the catalytic lifetime decreased with increasing H_2O/SiO_2 ratios in the precursors, which could be associated with the physicochemical properties, while the hydrocarbon selectivities were roughly the same.

Acknowledgements

This work was supported by the National Natural Science Foundation of China (Grant No. 21276183).

Appendix A. Supplementary data

Supplementary data related to this article can be found at http://dx.doi.org/10.1016/j.crci.2016.07.005.

References

[1] G. Luo, A.G. McDonald, Energy Fuels 28 (2014) 600.
[2] U. Olsbye, S. Svelle, M. Bjørgen, P. Beato, T.V.W. Janssens, F. Joensen, S. Bordiga, K.P. Lillerud, Angew. Chem., Int. Ed. 51 (2012) 5810.
[3] M. Stöcker, Micropor. Mesopor. Mater. 29 (1999) 3.
[4] M. Boltz, P. Losch, B. Louis, Adv. Chem. Lett. 1 (2013) 247.
[5] S.K. Saxena, N. Viswanadham, A.H. Al-Muhtaseb, J. Ind. Eng. Chem. 20 (2014) 2876.
[6] Q. Wang, S. Xu, J. Chen, Y. Wei, J. Li, D. Fan, Z. Yu, Y. Qi, Y. He, S. Xu, C. Yuan, Y. Zhou, J. Wang, M. Zhang, B. Su, Z. Liu, RSC Adv. 4 (2014) 21479.
[7] D.P. Serrano, J.M. Escola, P. Pizarro, Chem. Soc. Rev. 42 (2013) 4004.
[8] B. Liu, L. Zheng, Z. Zhu, K. Zhang, H. Xi, Y. Qian, RSC Adv. 4 (2014) 13831.
[9] S. Mintova, M. Jaber, V. Valtchev, Chem. Soc. Rev. 44 (2015) 7207.
[10] S. Fathi, M. Sohrabi, C. Falamaki, Fuel 116 (2014) 529.
[11] Y. He, M. Liu, C. Dai, S. Xu, Y. Wei, Z. Liu, X. Guo, Chin. J. Catal. 34 (2013) 1148.
[12] J. C. Kuo, US Patent 3,931,349, 1976.
[13] J. Robert, W. Keading, US Patent 3,702,886, 1972.
[14] X. Wang, X. Gao, M. Dong, H. Zhao, W. Huang, J. Energy Chem. 24 (2015) 490.
[15] A. Petushkov, S. Yoon, S.C. Larsen, Micropor. Mesopor. Mater. 137 (2011) 92.
[16] S. Narayanan, J.J. Vijaya, S. Sivasanker, L.J. Kennedy, S.K. Jesudoss, Powder Technol. 274 (2015) 338.
[17] H. Tao, H. Yang, X. Liu, J. Ren, Y. Wang, G. Lu, Chem. Eng. J. 225 (2013) 686.
[18] L. Chen, S.Y. Zhu, Y.M. Wang, M.-Y. He, New J. Chem. 34 (2010) 2328.
[19] Z. Deng, Y. Zhang, J. Zheng, K. Zhu, X. Zhou, New J. Chem. 39 (2015) 7777.
[20] Z. Wan, W. Wu, W. Chen, H. Yang, D. Zhang, Ind. Eng. Chem. Res. 53 (2014) 19471.
[21] A.A. Rownaghi, F. Rezaei, J. Hedlund, Catal. Commun. 14 (2011) 37.
[22] M. Choi, K. Na, J. Kim, Y. Sakamoto, O. Terasaki, R. Ryoo, Nature 461 (2009) 246.
[23] G. Majano, A. Darwiche, S. Mintova, V. Valtchev, Ind. Eng. Chem. Res. 48 (2009) 7084.
[24] E. Koohsaryan, M. Anbia, Chin. J. Catal. 37 (2016) 447.
[25] F. Meng, Y. Wang, S. Wang, RSC Adv. 6 (2016) 58586.
[26] T. Xue, L. Chen, Y.M. Wang, M.-Y. He, Micropor. Mesopor. Mater. 156 (2012) 97.
[27] G. Wu, W. Wu, X. Wang, W. Zan, W. Wang, C. Li, Micropor. Mesopor. Mater. 180 (2013) 187.
[28] Y. Tang, B. Li, N. Zhang, S. Wang, Y. Wen, P. Jin, X. Wang, CrystEngComm 14 (2012) 3854.

[29] F. Xu, M. Dong, W. Gou, J. Li, Z. Qin, J. Wang, W. Fan, Micropor. Mesopor. Mater. 163 (2012) 192.
[30] Q. Yu, X. Meng, J. Liu, C. Li, Q. Cui, Micropor. Mesopor. Mater. 181 (2013) 192.
[31] M. Razavian, S. Fatemi, Mater Chem. Phys. 165 (2015) 55.
[32] M. Razavian, S. Fatemi, M. Komasi, Mater Res. Bull. 65 (2015) 253.
[33] N. Ren, J. Bronić, B. Subotić, X.-C. Lv, Z.-J. Yang, Y. Tang, Micropor. Mesopor. Mater. 139 (2011) 197.
[34] N. Ren, J. Bronić, B. Subotić, Y.-M. Song, X.-C. Lv, Y. Tang, Micropor. Mesopor. Mater. 147 (2012) 229.
[35] Q. Zhang, S. Hu, L. Zhang, Z. Wu, Y. Gong, T. Dou, Green Chem. 16 (2014) 77.
[36] T. Zhang, Y. Wang, S. Wang, X. Wu, P. Yao, W. Feng, Y. Lin, J. Xu, React. Kinet. Mech. Catal. 114 (2015) 735.
[37] A.E. Persson, B.J. Schoeman, J. Sterte, J.E. Otterstedt, Zeolites 14 (1994) 557.
[38] N. Ren, Z.-J. Yang, X.-C. Lv, J. Shi, Y.-H. Zhang, Y. Tang, Micropor. Mesopor. Mater. 131 (2010) 103.
[39] N. Ren, J. Bronić, T.A. Jelić, A. Palčić, B. Subotić, Cryst. Growth Des. 12 (2012) 1736.
[40] L. Wang, P. Tian, Y. Yuan, M. Yang, D. Fan, H. Zhou, W. Zhu, S. Xu, Z. Liu, Micropor. Mesopor. Mater. 196 (2014) 89.
[41] Z. Gabelica, N. Blom, E.G. Derouane, Appl. Catal. 5 (1983) 227.
[42] E.G. Derouane, Z. Gabelica, J. Solid State Chem. 64 (1986) 296.
[43] A.E. Persson, B.J. Schoeman, J. Sterte, J.E. Otterstedt, Zeolites 15 (1995) 611.
[44] D. Kistamurthy, A.M. Saib, D.J. Moodley, J.W. Niemantsverdriet, C.J. Weststrate, J. Catal. 328 (2015) 123.
[45] C.G. Granqvist, R.A. Buhrman, J. Catal. 42 (1976) 477.
[46] J. Datka, B. Sulikowski, B. Gil, J. Phys. Chem. 100 (1996) 11242.
[47] J. Liu, G. Jiang, Y. Liu, J. Di, Y. Wang, Z. Zhao, Q. Sun, C. Xu, J. Gao, A. Duan, J. Liu, Y. Wei, Y. Zhao, L. Jiang, Sci. Rep. 4 (2014) 7276.
[48] J. Zhang, W. Qian, C. Kong, F. Wei, ACS Catal. 5 (2015) 2982.
[49] M. Firoozi, M. Baghalha, M. Asadi, Catal. Commun. 10 (2009) 1582.
[50] T. Ge, Z. Hua, X. He, Y. Zhu, W. Ren, L. Chen, L. Zhang, H. Chen, C. Lin, H. Yao, J. Shi, Chin. J. Catal. 36 (2015) 866.
[51] Q. Wang, Y. Wei, S. Xu, M. Zhang, S. Meng, D. Fan, Y. Qi, J. Li, Z. Yu, C. Yuan, Y. He, S. Xu, J. Chen, J. Wang, B. Su, Z. Liu, Chin. J. Catal. 35 (2014) 1727.
[52] J. Ahmadpour, M. Taghizadeh, C. R. Chimie 18 (2015) 834.